EPITAXIAL LATERAL OVERGROWTH TECHNIQUE – BASICS OF THE GROWTH TECHNOLOGY AND PROPERTIES OF THE LAYERS

Zbigniew R. Zytkiewicz

Institute of Physics, Polish Academy of Sciences,
Al. Lotnikow 32/46, PL-02-668 Warszawa, Poland.
e-mail: zytkie@ifpan.edu.pl

ABSTRACT

This article provides a general review of the epitaxial lateral overgrowth (ELO) technology and of application of ELO layers as substrates with adjustable value of lattice constant. In particular, the issues of ELO growth mechanism, substrate defect filtration during ELO procedure and strain in ELO layers will be addressed. Literature data on MOVPE and HVPE ELO growth of GaN on sapphire and our results on lateral overgrowth of III-V structures (GaAs/GaAs, GaAs/Si, GaSb/GaSb, GaSb/GaAs, etc.) by LPE are used as examples. Other lateral overgrowth techniques (LPE growth of lattice mismatched bridge layers and pendeo-epitaxy) will also be shortly presented and compared with the conventional ELO technique.

INTRODUCTION

The possibility of growing high-quality epitaxial layers of different materials on lattice mismatched substrates is a topic of considerable interest. The range of useful devices available with a given substrate is largely enhanced by this method. However, if epitaxial layer and substrate are not matched together, either by lattice constants, or by thermal expansion coefficients, dislocations can be generated at the interface. Segments of those dislocations propagating to epilayer surface (so-called *threading dislocations*) significantly deteriorate parameters of devices made of such heterostructures and enhance their degradation. Therefore, there is a continuous effort for better control of lattice misfit relaxation processes and reduction of defect density in of lattice mismatched structures. The most common approach is to use a buffer layer with graded or abrupt composition profile deposited on available substrate to obtain the layer with required value of lattice constant. However, despite sophisticated methods of buffer layers engineering, density of dislocations threading to the surface of the buffer from its interface with a lattice mismatched substrate is often still too high for device applications. Indeed, the best lattice-mismatched planar layers exhibit dislocation densities in the range of 10^6 – 10^7 cm^{-2}. Therefore, the lateral growth techniques have been developed to avoid propagation to the epilayer of dislocations present in the buffer layer.

Epitaxial lateral overgrowth (ELO) is a method of epitaxial growth on partially masked substrate [1]. Prior to the ELO procedure a suitable relaxed buffer layer is grown on the substrate. Then, the structure is covered by a thin masking film and patterned by conventional photolithography to form on its whole area a grating of mask-free seeding windows [Fig. 1(a)].

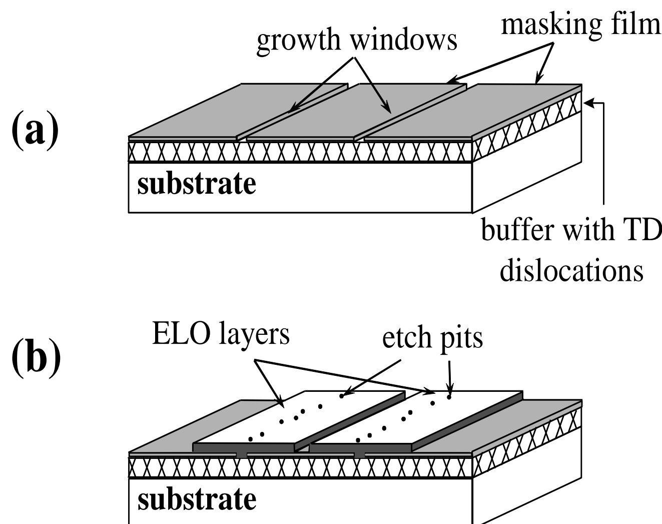

Fig.1. Principle of ELO procedure: (a) growth of relaxed buffer layer followed by deposition of an amorphous masking film, photolithography and etching of mask-free seeds ("growth windows"); (b) growth of ELO layers starts selectively from the seeds. Then, the ELO layers spread laterally over the masking film. TD are the dislocations threading to the surface of the buffer. The respective etch pits are visible on ELO surface over the seeds, only.

Finally, an ELO layer is deposited on such substrate. The epilayer nucleates on the seeds and the growth proceeds in the direction normal to the substrate. As soon as the crystallization front exceeds the top surface of the mask, the growth in lateral direction over the masking film starts [Fig. 1(b)]. The adjacent ELO stripes coalesce to form a continuous epilayer if enough growth time is given. Main advantage of this approach is that the buffer dislocations are blocked by the masking film and can propagate to the ELO layer through a narrow window in the mask, only. Therefore, the laterally grown parts of ELO layers (“wings”) should be nearly defect-free despite a high density of threading dislocations (marked as TD in Fig.1) in the underlying structure. As will be presented below, there are many experimental data showing high efficiency of defect filtration in epitaxial laterally overgrown semiconductor structures. Thus, the ELO method, when combined with well elaborated techniques of buffer layers engineering, is a promising tool to grow high quality epilayers on available lattice mismatched substrates. Then, required value of lattice constant is obtained by controlling composition of the buffer, while dislocations introduced during relaxation of its lattice mismatch with the substrate are filtered during subsequent homoepitaxial lateral overgrowth. In this way new semiconductor substrates with lattice constant different from that of available bulk III-V crystals can be generated allowing for epitaxy of a new class of high quality semiconductor structures required by modern opto- and microelectronics. The recent breakthrough in development of long lifetime GaN/InGaN blue lasers, being due to the high efficiency of defects filtration during lateral growth, is the most spectacular recent achievement of the ELO technique [2].

Two main fields of interest can be easily distinguished in the published reports on ELO research. These are lateral overgrowth of GaN epilayers on sapphire or SiC substrates and ELO of “traditional” III-V compounds (e.g. GaAs or InP) on silicon substrates. This choice apparently results from the market demand for novel, low cost semiconductor devices. Therefore, vapor phase growth of ELO GaN and liquid phase epitaxial lateral overgrowth of GaAs and GaSb will be used as examples in this review to illustrate the basic phenomena that take place in ELO structures. We will show that some general rules for growing of thin and wide layers, efficient filtration of defects threading from underlying buffer and impact of this proces on structural and optical quality of overgrown material, interaction of ELO layers with the mask leading to downward wings tilt and the ways this tilt can be reduced, relaxation of thermal stress via wing tilting – all these phenomena are similar in both cases despite fundamental differences between the growth techniques used and different properties of materials grown. This clearly means that they are not specific attributes of particular ELO case but must originate directly from the principle of the ELO technique. Presentation of such general features of epitaxial lateral overgrowth is the aim of this article. In the following sections the issues of ELO growth mechanism, substrate defects filtration during ELO procedure and strain in ELO layers will be addressed.

1. Mechanism Of Growth Of ELO Layers

In general, the sharp interfaces between liquid and solid phases can be classified in three groups, namely perfect singular, imperfect singular and rough [3]. Fig. 2 shows schematically the dependence of growth rate on interface supersaturation for those three types of interface.

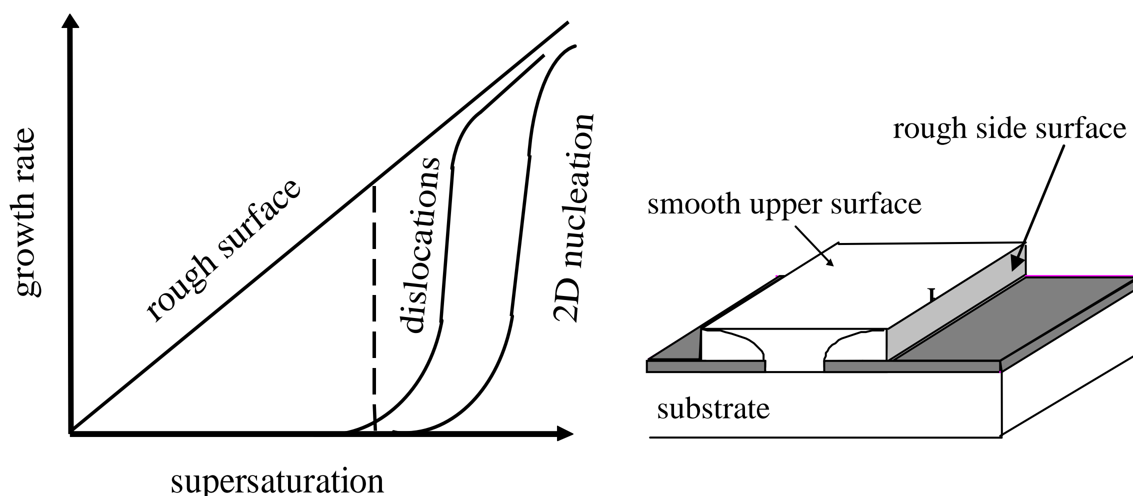

Fig.2. Dependence of growth rate on supersaturation for selected growth modes. It is recommended to grow the ELO layers at low supersaturations as indicated by dashed line. Then, large growth anisotropy between sides ELO walls (rough) and upper ELO surface (smooth) can be obtained.

On a perfect singular face the atoms can be incorporated to solid in the form of two-dimensional nuclei only. This requires some energy to create stable nucleus larger than the critical one. If the interface is singular but imperfect, the surface irregularities (e.g. dislocations) supply the steps necessary for lateral growth from them. In the case of rough interface atoms can be added to the face in a random way and the growth rate varies linearly with the interface supersaturation. As discussed by Nishinaga [4] the basic idea of ELO lies in fundamental dissimilarities between those growth modes. If a slowly grown facet of (100) - or (111)-type covers the upper plane of ELO whereas the side walls are atomically rough, then a large growth rate difference in vertical and horizontal directions can take place. As seen from Fig. 2, a low supersaturation of the liquid phase (as marked by vertical dashed line in the figure) is required for the successful ELO growth. Then a large anisotropy of ELO layers can be obtained.

To benefit from natural growth anisotropy of various crystals faces the ELO process should proceed at low supersaturation [4]. Therefore, equilibrium growth techniques as liquid phase epitaxy (LPE) or vapor phase epitaxy (VPE) should be chosen, if possible, for lateral overgrowth. Indeed, the ELO layers with the value of the aspect (wing width/thickness) ratio as large as 120 are actually grown from a liquid phase (see Fig.3). Solution or melt growth of group III nitrides is extremely complicated due to low solubility of nitrogen in liquid metals. Therefore, metalorganic VPE (MOVPE) or hydride VPE (HVPE) is commonly used nowadays to grow ELO structures of these compounds.

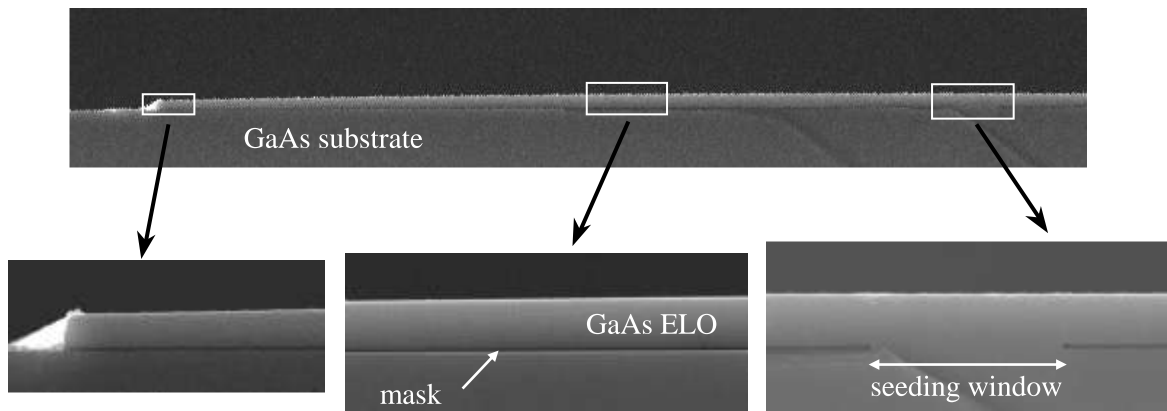

Fig.3. By careful adjustment of growth conditions very thin and wide ELO layers can be grown by LPE. As example, figure shows cross-section of GaAs ELO layer grown by LPE on SiO_2-masked GaAs substrate. The layer is 354 μm wide and μm thick.

However, large supersaturation at the growing face makes control of growth anisotropy difficult, so lateral structures of GaN with aspect ratio up to 4 are obtained by MOVPE, only. Molecular beam epitaxy (MBE) growth of ELO layers is even more complicated as deposition of polycrystalline material on the mask is hard to avoid [5, 6]. Sophisticated systems with molecular beams oriented at low angle to the substrate, low growth rate and precise temperature control [7] or special substrate preparation and growth procedures [8] are necessary to get growth started selectively from the seed. There is no significant gas phase diffusion during MBE growth, so lateral overgrowth must rely on the surface mobility of adatoms, only. Therefore, even if growth selectivity is obtained, the MBE grown ELO layers are usually very narrow which makes their application in devices production difficult.

Much is known already about the mechanisms active during growth of ELO layers (see Refs. [4] and [9] for a review). It has been shown that shape of cross-section and the aspect ratio of the layers can be efficiently controlled by choice of seed orientation. The basic idea is to find such orientation of the seeding lines for which fast-growing planes cover the side walls of the ELO layer, while the slowly grown facet is formed on the upper surface. Then, the requirement of large ratio of lateral to vertical growth rates can be fulfilled [4]. For GaN on sapphire ELOs the seeding windows are usually aligned along the <11-20> or the <1-100> directions of GaN [10]. For LPE growth of ELO layers on (100) GaAs or InP substrates seeding lines with directions slightly rotated relative to the <110> are commonly used [4]. Steps on the surface supplied by substrate miscut or dislocations enhance the vertical growth of ELO [9, 11]. Therefore, additional restriction for seeds direction appears on off-oriented substrates. Then, from the optimal seed directions the one must be chosen for which density of misorientation steps inside the seeding area is the smallest [11]. For the same reason dislocation density in the buffer must be as low as possible to obtain ELO layers with a large value of the aspect ratio. For a given geometry of ELO mask, control of surface supersaturation is usually done by varying growth temperature, initial melt supersaturation and cooling rate in LPE. Available experimental data [9, 12-16] as well as numerical simulations [17-19] show that low supersaturation of liquid phase and slow cooling are preferred for growing wide and thin ELO layers. Doping

has also been found as a useful way by which the vertical growth rate can be reduced, leading to thin and wide ELO layers. Indeed, we have reported a significant increase of the width/thickness ratio for heavily Si doped GaAs ELO layers grown by LPE [20]. The effect has been explained as being due to impurity induced retardation of surface steps flow on the upper surface of ELO. Similar phenomenon has also been found for Mg-doped GaN ELO layers grown by MOVPE [21].

2. Filtration Of Substrate Defects In ELO Structures

Figure 4(a) shows scanning electron microscopy (SEM) image of cross-section of GaAs ELO layer deposited on silicon substrate. The structure consists of (100) Si substrate with MBE grown 2 μm thick GaAs buffer on which the SiO_2 masking film has been sputtered. The GaAs ELO layer was grown by LPE. Its width and thickness are 85 μm and 11 μm, respectively. Other growth details can be found elsewhere [22]. Figure 4(b) shows plane view of the same layer after revealing etch pits by etching in molten KOH. It is noticing worthy that density of etch pits on the buffer surface is very high (~ 10^8 cm^{-2}). On the contrary, in the ELO layer only the dislocations threading from the buffer are observed. As shown in Fig. 4(a), these dislocations are confined in a very narrow area above the seed. The rest of the ELO layer is nearly dislocation free, which has been additionally proved by studies of the layers with the use of synchrotron x-ray topography technique [23]. The same behavior is seen in Figs. 4(c)-(d) for GaSb/GaAs structure.

Fig.5 shows cross-section of GaAs/Si ELO structure as seen in transmission electron microscopy (TEM). In agreement with previous discussion it is seen that buffer dislocations propagate to the ELO layer through the seeding area only, without access to the laterally grown parts of the layer. Note also that these dislocations are of 60°-type. They are inclined to the interface plane, so width of the defected zone increases with the layer thickness. This finding explains why it is so important to keep the ELO layer thin. If lateral growth rate is increased at expense of vertical growth a large dislocation-free area of the layer can be obtained [24].

The images presented in Figs. 4 and 5 are the best evidences that that the mechanism of substrate defects filtration active during ELO procedure is very efficient. This phenomenon is commonly observed in laterally overgrown semiconductor structures of other materials [4, 25-27].

High crystallographic quality of ELO wings results in their better optical properties than that of planar buffers. As example, Figure 6 shows plane view of the GaAs on Si ELO structure similar to that from Fig. 4(a), in panchromatic mode of cathodoluminescence (CL). Higher CL intensity from the wing as compared to that coming out from the material grown vertically above the seed, and even much higher than that coming out from the buffer, is clearly visible. This is what should be expected, as dislocations are known to behave like centres of effective non-radiative recombination of excited carriers. Similar distribution of cathodoluminescence intensity has also been observed across surface of GaN on sapphire ELO structures [28].

An advantage of using ELO layers for epitaxial device structures was first demonstrated by Nakamura et al., who reported in 1997 a multiquantum well InGaN/GaN laser diode having a life-time longer than 1000 hr when deposited on GaN/sapphire ELO substrate [29]. Since then the life-time of these diodes has been significantly increased, so they are commercially available at present. For a comparison, the same InGaN/GaN diodes made on conventional sapphire substrates had worked for 300 hr, only [30]. This

remarkable improvement was due to significant reduction of the threshold current density of the laser diodes fabricated on low dislocation density ELO substrates. Kozodoy et al. have shown directly that the use of lateral overgrowth to eliminate dislocations leads to better electrical properties of GaN p-n junctions [31]. Reverse-bias leakage current was reduced by three orders of magnitude for the diodes located on low-dislocation density ELO wings. Moreover, large reduction of dark current and sharper cutoff have been found for AlGaN solar-blind detectors fabricated on ELO substrates [32]. The examples presented above are the best evidences that application of ELO technology leads to significant progress in development of high performance semiconductor devices made of lattice mismatched epitaxial structures.

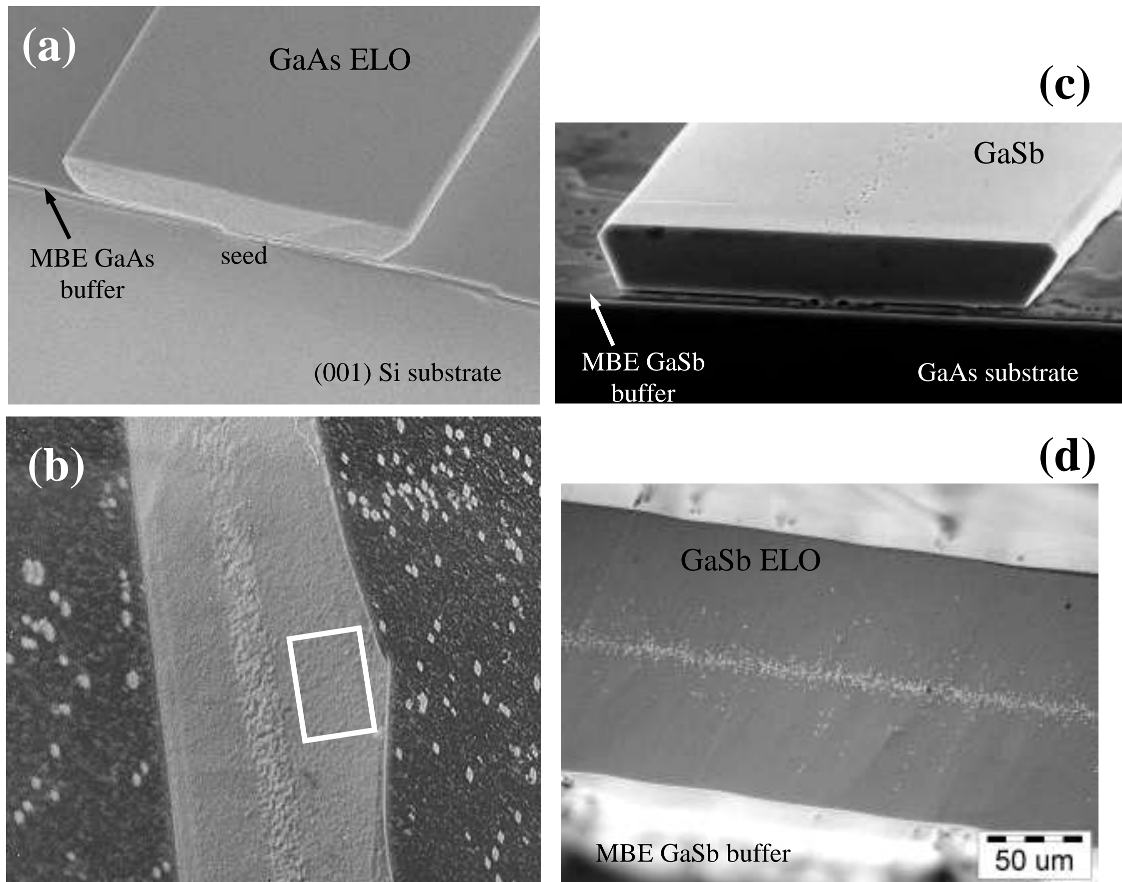

Fig.4. Scanning electron microscopy mages of GaAs/Si (a-b) and GaSb/GaAs (c-d) ELO structures; (b) and (d) are plane view images after etching of structures in KOH to reveal etch pits distribution on upper surfaces. Note that dislocation termination points are located above the seeding area only. The laterally grown parts exhibit low density of defects despite a high dislocation density in the buffer layer under the mask (visible outside the ELO stripe in (b)). If ELO layers are to be used as substrates for device structures the devices should be located in low-dislocation density area, as marked by white line in (b).

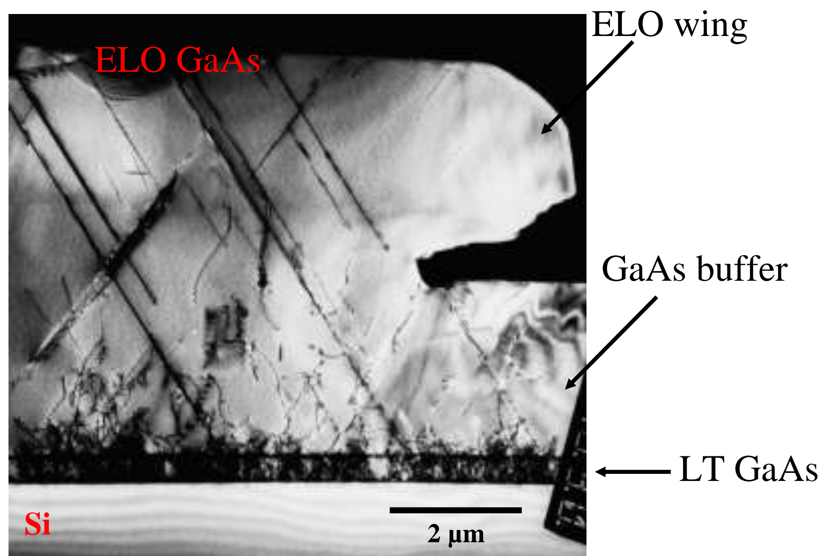

Fig.5. TEM cross-section image of LPE grown GaAs on Si ELO structure. Note from the bottom: Si (001) substrate, thin layer of GaAs grown at low temperature (LT GaAs), GaAs buffer and GaAs ELO layer. Dislocations from the buffer propagate to the ELO in the middle, mask-free area of the substrate. Laterally grown parts ("wings") of ELO exhibit much lower dislocation density than MBE grown GaAs

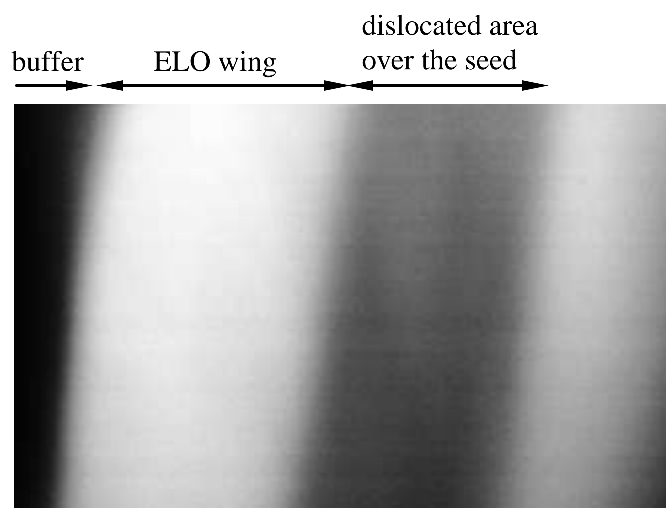

Fig.6. Cathodoluminescence image of LPE grown GaAs on Si ELO structure from Fig.

3. Strain In ELO Structures

As shown in previous sections of the paper ELO layers are of much higher quality than the reference planar structures but they are not free of strain. In particular, there is a question about strain induced by the mask itself and/or its possible interaction with the overgrown layer. Moreover, the lattice mismatch and thermal strain induced by different thermal expansion coefficients of subsequent layers and the substrate may result in large deformations of the layers. Although in real heteroepitaxial ELO structures all these phenomena are present together, for clarity of presentation in the next section problem of interaction of ELO layers with the mask underneath will be discussed first. Then, the issue of thermal strain in ELO structures will be addressed.

X-ray diffraction and topography techniques are commonly employed when studying strain in laterally overgrown structures. Figure 7 shows the typical geometry used for measurements of x-ray rocking curves of ELO layers. First, the rocking curve is measured for the sample position in which the scattering plane (defined by incident and diffracted wave vectors) is perpendicular to the seeding line direction. This corresponds to the axis of sample rotation during the ω scan being parallel to the seeds ($\varphi = 0$). Next, the sample is rotated around the substrate normal and the rocking curve is measured again for the scattering plane perpendicular to the seeds (i.e., for $\varphi = 90^o$). As will be shown later, this procedure allows determining the most characteristic features of the strain field in the samples.

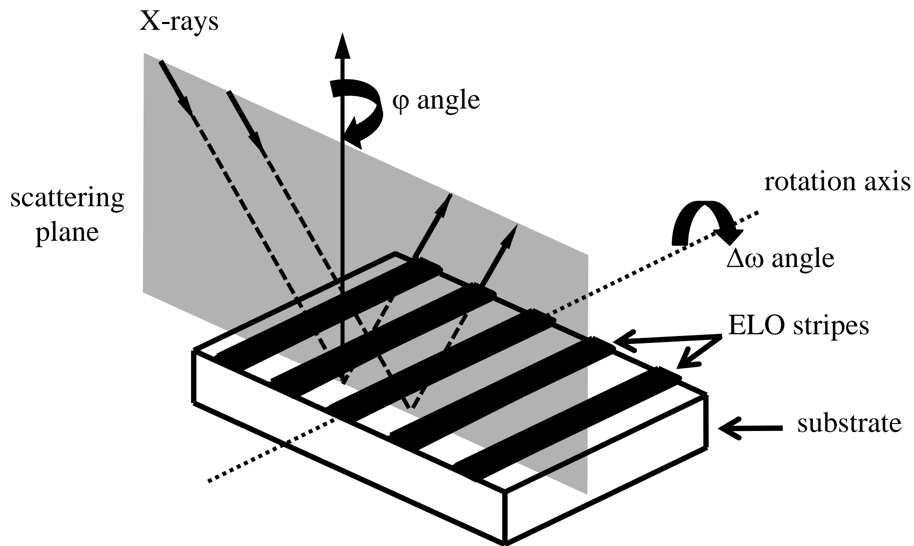

Fig.7. Schematic of geometry used for measurements of x-ray rocking curves of ELO samples. The scattering plane (marked in grey) is defined by incident and diffracted wave vectors. φ is the angle between direction of the seeds and the sample rotation axis during the ω scan; $\varphi = 0^o$ for the geometry shown.

3.1. Mask Induced Strain In ELO Layers

Figure 8 shows x-ray rocking curves of GaAs layer grown by LPE on SiO_2 masked GaAs substrate (see the source article for growth details) [33]. Both, the as-grown sample and that cut from the same wafer and etched to remove selectively the SiO_2 mask have been studied. The rocking curves presented in Figs. 8(a) and 8(b) have been measured with the $\varphi = 0^o$ and $\varphi = 90^o$ sample orientation, respectively. As it can be seen from Fig. 8(a) the rocking curve of the as-grown sample is very broad. However, it becomes much narrower after the SiO_2 mask has been removed. On the contrary, for $\varphi = 90^o$ the rocking curve is quite narrow and etching causes only a slight change of its shape [Fig. 8(b)]. It is worth mentioning that during rocking curve measurements the x-ray diffraction is sensitive mainly to the distortion of the (100) crystal planes in the scattering plane. Therefore, the large width of the rocking curve shown in Fig. 8(a) indicates that a significant deformation of the as-grown ELO takes place in the cross-section plane perpendicular to the seeds. In principle, similar broadening of the rocking curve could also be caused by lattice mismatch and/or composition gradients inside the structure. However, our analysis of reciprocal space maps collected during diffraction experiments of the same sample has ruled out such possibilities in our case [34].

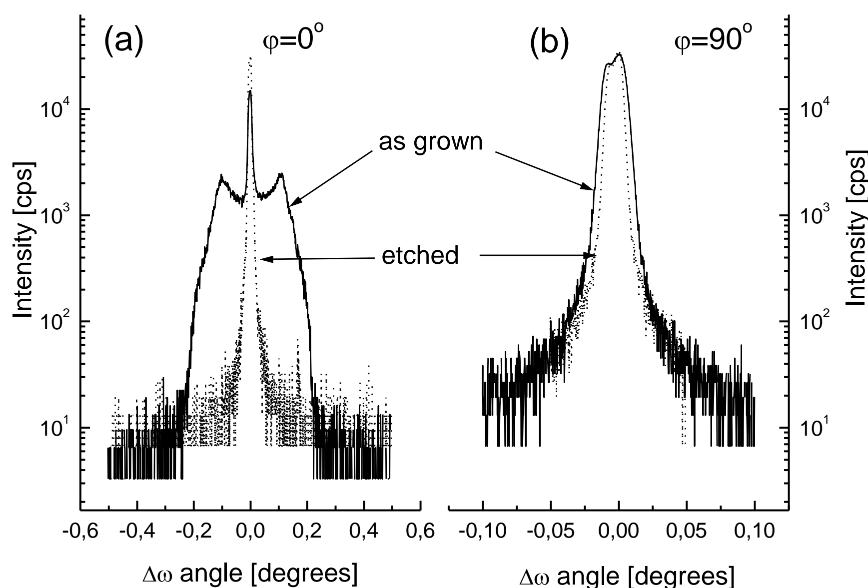

Fig.8. X-ray rocking curves of (400) $CuK\alpha_1$ reflection from the as-grown (solid line) and etched (dotted line) GaAs ELO layers on the SiO_2 -covered GaAs substrate measured with the ω axis parallel (a) and perpendicular (b) to the seeding lines.

We have postulated the following picture of strain in GaAs ELO layers grown by LPE on GaAs substrates [33]: the layers are under stress due to interaction of ELO wings with the SiO_2 mask. This stress is below the plastic flow threshold and accompanied strain, responsible for downward tilt of ELO wings visible in Fig. 9(a), disappears when the SiO_2 mask is removed by selective etching [Fig. 9(b)]. Let us to point out that from the shape of the rocking curve alone it is impossible to say whether the ELO wings tilt upwards or downwards, so additional experiments are needed to determine unambiguously the tilt

direction. In our case, we did a series of diffraction experiments in which a very narrow x-ray beam was precisely moved in small steps across a wide GaAs ELO layer [35]. Thus, measurements of rocking curves from precisely defined regions of the single ELO stripe were possible. By analyzing the order in which the side maxima appear while the beam is moved across the stripe we have proved that the wings tilt towards the mask surface. Moreover, the data obtained by scanning x-ray diffraction experiments were used to explain the origin of all the features visible on the rocking curve in Fig. 8(a). In particular, we have proved that the side maxima are due to diffraction from the edges of the ELO stripe. Therefore, the misorientation of ELO crystal planes must be the largest there. Consequently, half of the angular separation of the side peaks on the rocking curve can be used as a good measure of the maximum tilt angle $\Delta\Theta_{max}$ of ELO lattice planes [see Fig. 9(a)].

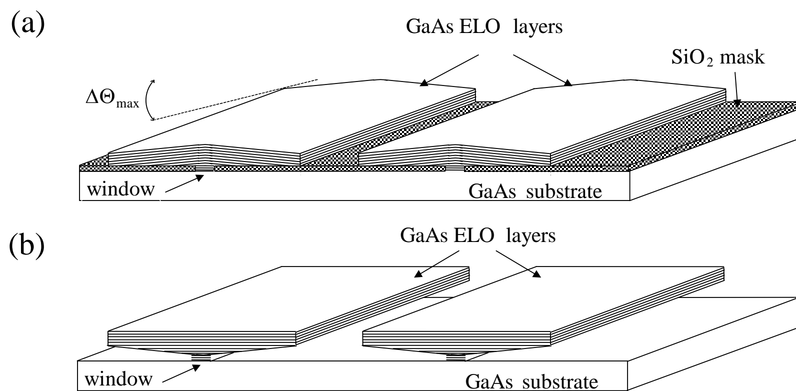

Fig.9. Schematic drawing of the GaAs on GaAs ELO cross-section. Bending of the layers is shown in the as-grown state (a). The deformation of crystal planes disappears when the SiO_2 mask is removed by etching (b). $\Delta\Theta_{max}$ is the tilt angle of (100) crystal planes between the edge and the central part of ELO.

We have studied the homoepitaxial GaAs ELO layers by synchrotron x-ray reflection and transmission topography techniques [23, 36-38]. The data obtained fully confirm the picture of strain in ELO structures shown in Fig. 9. The topographs together with appropriate numerical simulations have also been used to determine quantitatively how the misorientation of ELO lattice planes varies with position across the ELO stripe [37]. This procedure has led us to the conclusion that misorientation of the ELO lattice planes increases much faster near the centre of the ELO stripe than at the edges. In other words, the curvature radius of (100) lattice planes increases towards the edges of the ELO layer, which is in a very good agreement with the measured shape of the ELO surface. Such analysis of ELO lattice planes curvature has allowed us to postulate that bending of the ELO stripes starts at the very beginning of growth when the laterally overgrown parts are thin and flexible. Then, the bent crystal planes might be reproduced during subsequent growth, though still retaining their shape [37].

Very broad x-ray rocking curves similar to that shown in Fig. 8(a) are very often observed in various ELO systems, which shows that tilting of ELO wings towards the mask is a common problem in laterally overgrown structures. In some cases (e.g. in GaN on

sapphire ELO structures) the values of the tilt angle $\Delta\Theta_{max}$ in excess of 2° are reported [39]. So large tilts cannot be accommodated elastically, i.e. by the mechanism we have observed in our GaAs/GaAs samples [see Figs. 8(a) and 9(b)]. Indeed, cross-sectional transmission electron microscopy studies of GaN on sapphire ELO structures have revealed characteristic defects in the overgrown region, which consisted of arrays of dislocations running along the seed direction [40]. These defects, originating from the bent TD dislocations propagating laterally in the ELO layer, create a low-angle tilt boundaries above the edges of the SiO_2 mask.

Tilting of wings caused by their interaction with the mask underneath creates significant problems for coalescence of neighboring stripes as they tilt in opposite directions [see Fig. 9(a)]. As example, Fig. 10 shows TEM cross-section image of coalescence front of two GaAs ELO stripes grown on GaAs substrate from adjacent seeding lines. Creation of dislocation network to accommodate opposite tilt of neighboring stripes is clearly visible. The same phenomenon we have observed by cathodoluminescence imaging of upper surface of joining ELO layers. Similar behavior has been also observed for GaN on sapphire fully overgrown ELO structures [40]. The image presented in Fig. 10 clearly shows how serious degradation of ELO quality can be caused by tilting of laterally overgrown parts of the layers. Therefore, there is a widespread discussion in the literature on the origin of tilting of the ELO wings and on the way in which it can be reduced by controlling the growth parameters.

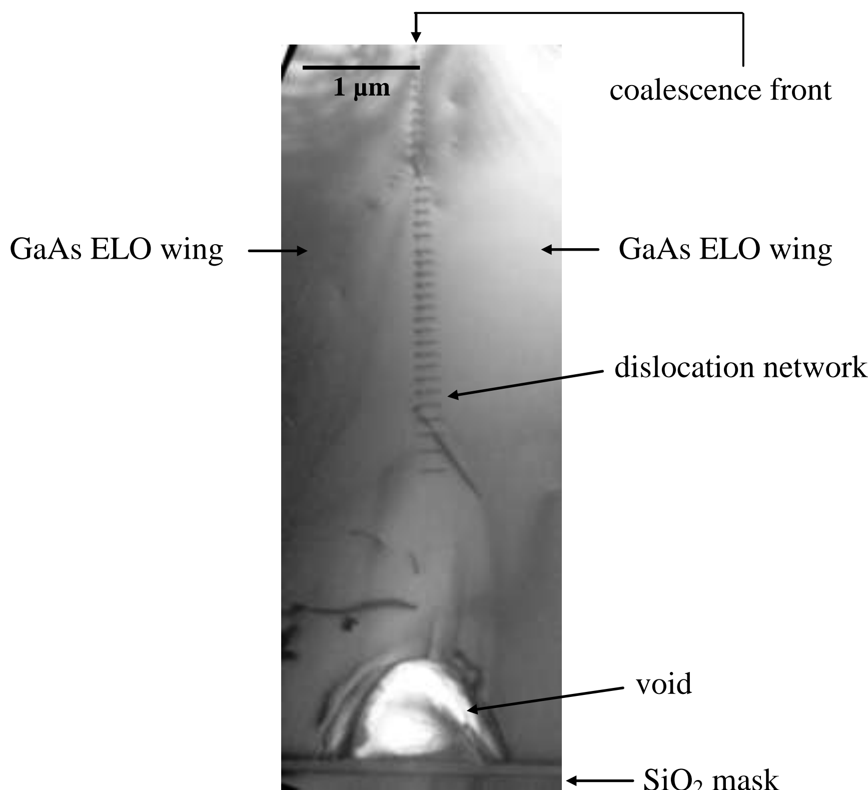

Fig.10. TEM image of coalescence front of two GaAs ELO stripes grown on GaAs substrate from adjacent seeds. Note presence of void near the mask surface and the dislocation network accommodating misorientation of ELO lattice planes at the coalescence front.

Fini with co-workers were the first who used x-ray diffraction to observe the time evolution of lattice planes bending in GaN on sapphire ELO layers [41]. They have observed the (10-13) diffraction peak of GaN obtained in situ, during growth of the structures by MOVPE. The data collected during this elegant experiment is direct evidence that wing tilt must be due to interaction of the wing with the mask and that ELO wings tilt starts at the very beginning of lateral overgrowth, in agreement with our earlier suggestion [37].

Keeping this in mind the following recipe for the reduction of the mask-induced bowing of ELO layers can be proposed: the initial vertical growth rate of ELO must be increased to start the lateral overgrowth at some microscopic distance from the upper surface of the mask [35]. Then, the chance of ELO wings capture by attractive force and their interaction with the mask should be reduced. We have found several examples that this recipe efficiently works in practice. In particular, we have shown that the GaAs ELO layers grown on SiO_2 coated substrates are strain-free if their wings hang over without any contact with the underlying mask [42]. In the other cases, tilting of the wings can be efficiently tailored by controlling the ratio of vertical to lateral growth rates at the beginning of ELO growth. This has been achieved by growing the GaAs ELO layers on SiO_2-coated GaAs substrates with increasing density of dislocations. Then, the ratio of vertical to lateral growth rates at the beginning of the growth was increased due to the higher density of surface steps, which in turn led to reduction of the mask-induced tilt of ELO wings [35, 42]. In the limiting case of heavily dislocated GaAs substrates, namely on GaAs-coated Si substrates, the vertical growth of GaAs ELO was so fast that air-bridged structures without any interaction with the mask were obtained [22]. Similarly, Fini et al. have shown that the quality of coalescence of adjacent ELO GaN stripes can be improved by forcing vertical development of ELO stripes at the beginning of the growth, followed by change of growth conditions and fast lateral overgrowth of the structure [43]. This is exactly the same recipe we have proposed.

Replacement of commonly used dielectric films by other mask materials seems to be a promising way of reduction of mask induced wing tilt. In particular, we have found that that bending of the GaAs ELO layers grown by LPE is negligible when the SiO_2 mask is replaced by a thin graphite film [33]. We have explained this finding by delayed start of lateral growth caused by the change of the shape of the melt in the corner between the side wall of the ELO layer and the mask when the SiO_2 is replaced by graphite film not wetted by the gallium melt [42]. Similarly, tungsten has been found as promising mask material for MOVPE growth of GaN ELO structures with very low tilt of the wings [44]. In principle however, it is difficult to predict a priory the mask material that would be the most suitable for each particular ELO case. Therefore, the most natural way to eliminate the mask induced strain would be to grow the ELO structures with their wings having no direct contact with the mask surface. The GaN air-bridged ELO structures grown by Kidoguch et al. [45] or our GaAs ELO layers with wings hanging over the mask (see Fig.11) [42] are the best examples that this goal can be achieved. Unfortunately, quite often the growth conditions required for reproducible growth of such structures are difficult to find.

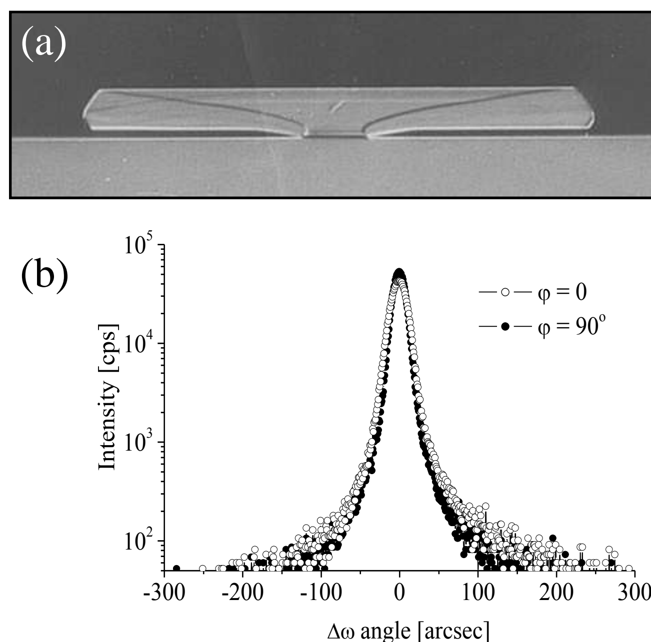

Fig.11. (a) cross-section of GaAs ELO layers with wings hanging over the SiO_2 masked GaAs substrate. X-ray rocking curves of the sample are narrow for both orientation of x-ray scattering plane (b), which indicates no tilt of the wings towards the mask.

3.2. Thermal Strain In ELO Structures

Additional deformation of ELO lattice planes may arise when the sample, due to the different thermal expansion coefficients of its components, experiences a large stress upon cooling from the growth to room temperature. This effect is commonly observed in planar heterostructures. As will be shown below, in ELO structures this strain can be relaxed via additional tilting of ELO wings while still preserving their high quality.

Figure 12 shows the (400) $CuK\alpha_1$ rocking curve of the GaAs ELO layer on the GaAs-coated Si substrate [22]. The scattering plane was set perpendicular to the seeds in this experiment. As it is seen, the rocking curve consists of two peaks which are separated by $\Delta\Theta$=216 arcsec. The whole rocking curve is so wide that presence of ELO deformation similar to that observed by us for GaAs ELO layer on GaAs substrate could be suspected. For the ELO GaAs on GaAs system we attributed broadening of the rocking curve to the bending strain induced by ELO stripes adhesion to the SiO_2 mask. Then, the tilt of wings disappeared after the mask had been removed. As seen in Fig. 12, the situation is quite opposite for the ELO GaAs on Si - the separation of the peaks increases ($\Delta\Theta$=250 arcsec) after removal of the mask by selective etching. Moreover, analysis of layer cross sections with the use of optical microscope has revealed a microscopic gap between the ELO and the masking film. Thus, the mask induced bending of lattice planes cannot explain the data obtained.

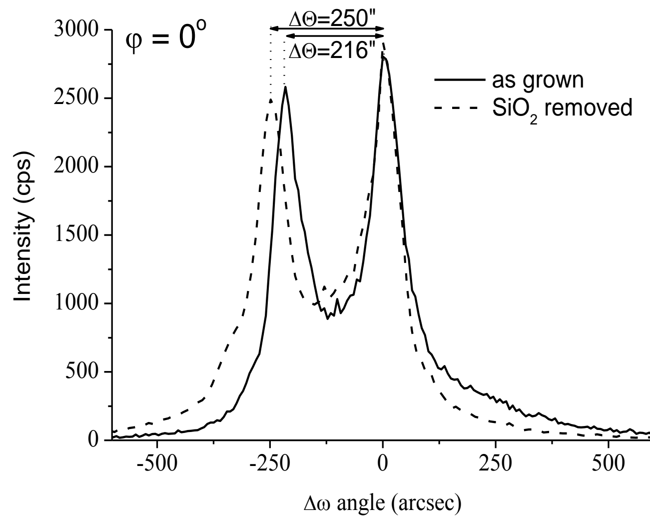

Fig.12. Rocking curves of (400) $CuK\alpha_1$ reflection for the as-grown (solid line) and etched (dotted line) GaAs ELO layer on the GaAs-coated Si substrate measured with the ω axis parallel to the seeding lines (φ=0).

We have performed x-ray diffraction experiments with a narrow x-ray beam moved across the single ELO stripe to show that two peaks visible in Fig. 12 are due to the diffraction from the wings. It is noticing worthy that the full width at half maximum of each peak equals to 94 arcsec only, which is much smaller than that of the MBE grown GaAs buffer (435 arcsec.). This result, together with an analysis of CL intensity (Fig. 6) and etch pits density [Fig. 4(b)] distributions, confirms very high crystallographic quality of laterally grown GaAs on Si substrates. By using x-ray diffraction technique with the beam scanned across the ELO layer we have proved also that the wings tilt upward in the GaAs on Si case [22], which is just opposite behavior to that observed in the GaAs/GaAs ELO system. All these results have allowed us to create a model of bending of the GaAs ELO layer on Si substrate as illustrated in Fig. 13. A biaxial tensile strain caused by different thermal contraction of epilayer and substrate is commonly observed in GaAs layers on Si substrates [46]. This strain disappears when the GaAs/Si structure is heated to the temperature ~500°C [47], which is close to our LPE growth temperature. Therefore, the GaAs ELO layer grows essentially stress free. At room temperature, the basal plane of the ELO should have the same tensile deformation as the upper surface of the buffer GaAs. Since the ELO layer stands free and does not adhere to the mask, unrestricted strain relaxation and free contraction of vertically grown volume of ELO should take place in its upper part. This, in turn, must lead to the upward bending of ELO wings (as shown in Fig. 13). The thermal tensile strain in the seeding area is partially compensated by the mask induced compression [34]. Therefore, deformation of ELO at its base, and consequently the ELO wings tilt angle, increase when the SiO_2 mask is removed. This leads to increase of angular separation of x-ray reflections as shown in Fig.12. Let us compare the rocking curves of the GaAs ELO layers grown on GaAs and GaAs-coated Si substrates shown in Figs. 8(a) and 12, respectively. The rocking curve from Fig. 8(a) is very broad which indicates some distribution of strain along the interface between the wing and the mask. On

the contrary, in the GaAs on Si structure strain is localized in the seeding area only and the main part of the wings is strain free, so the wing peaks are very sharp. In this way, the different shapes of the rocking curves directly reflect different mechanisms responsible for deformation of ELO lattice planes in both cases.

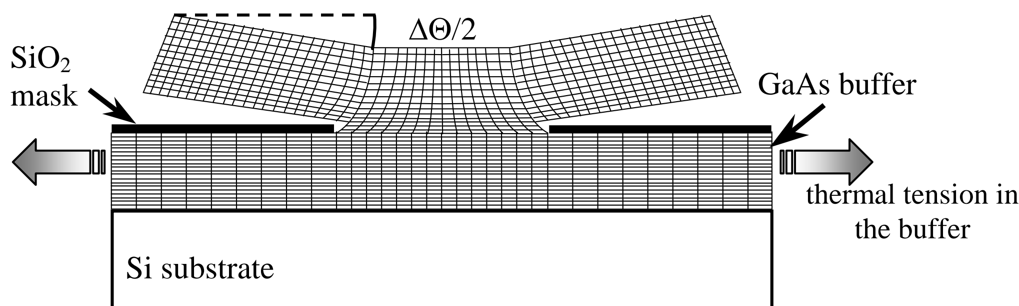

Fig.13. Schematic drawing of cross-section of the as-grown GaAs ELO layer on Si substrate. The tilt of (100) ELO wings crystal planes equals ΔΘ/2, where ΔΘ is angular separation of diffraction peaks in Fig. 12.

It is worthy noticing that our model of thermal strain relaxation in ELO layers predicts that the direction of wing tilt must be correlated with the sign of the strain in the buffer. In particular, downward wings tilt should be seen if the buffer layer is under compressive thermal stress (e.g. in GaN on SiC or sapphire substrates). This is exactly the behavior observed for the GaN on sapphire ELO system [41]. Qualitatively, the same phenomenon can be inferred from recent simulations via finite element analysis of strain in ELO structures [48].

4. Related Techniques Of Lateral Overgrowth

The most characteristic feature of the ELO process presented so far is the change of the predominant growth direction – from vertical in the growth window to lateral in the regions over the masking film. In principle however, it is possible to start lateral overgrowth from the seeds oriented perpendicular to the substrate surface, so change of the growth direction is not necessary. If the substrate (bare substrate or substrate covered by a suitable buffer layer) is etched to create on its surface a pattern of ridges or elongated columns orientated similar to that of windows in ELO, conditions are provided such that the side walls of the columns provide the crystallographic template for lateral growth.

Figure 14(a) shows geometry of silicon substrate used for LPE lateral overgrowth of Si from ridge seeds [49, 50]. A thin SiO_2 mask has been deposited in the trenches to avoid direct epitaxy on the substrate. During LPE the growth starts from the side walls of the ridges and proceeds laterally over the mask. The top surface of the ridge is the dislocation-free (111) Si facet, so it contains no step sources. Therefore, under proper growth conditions the vertical growth is completely eliminated and the layer grows laterally without any change of its thickness. As the thickness of the layer is determined by the ridge height, it can be easily controlled. However, very thin layers are difficult to obtain. When the thickness of the layer decreases the radius of curvature of its side wall decreases as well

[see Fig. 14(a)]. This leads to increase of the equilibrium concentration of the solute around this wall due to the Gibbs-Thomson effect. Therefore, higher melt supersaturation must be used to grow thinner layers. Then however, vertical growth may be initiated if the supersaturation is large enough for 2D nucleation at the top surface of the ridge. Using this technique as thin as 0.23 μm Si layers with the aspect ratio up to 82 have been grown laterally upon SiO_2-coated Si substrates by LPE [49].

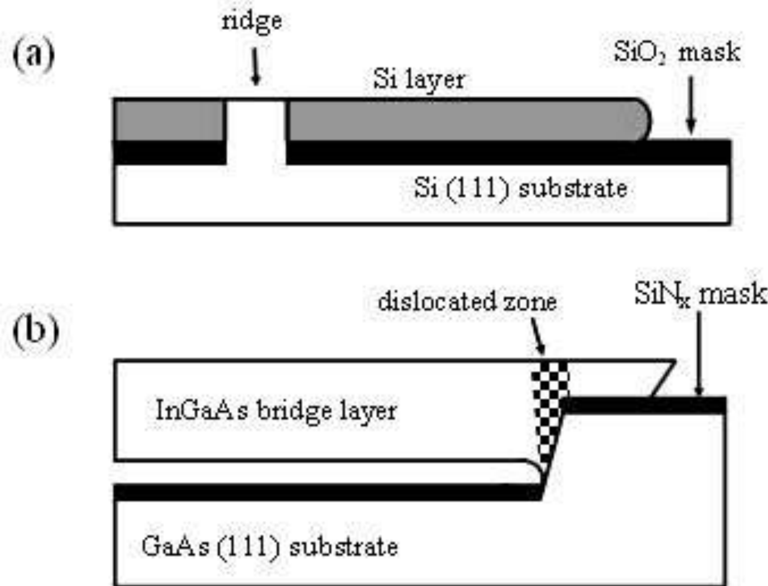

Fig.14. Schematic illustration of cross sections of Si epilayer grown on (111) Si substrate from a ridge seed (a) and of InGaAs bridge layer grown by LPE on GaAs (111) substrate (b).

On the contrary to the case of homoepitaxy, in lattice mismatched heterostructures the top surface of the columns is not dislocation-free and must be covered by an additional mask to avoid excessive vertical growth. Fig. 14(b) shows schematically how this approach has been applied by Iida et al. to grow by LPE InGaAs bridge layers on GaAs substrates [51]. First, the substrate covered by the SiN_x mask has been processed by photolithography and etching to fabricate on its surface a pattern of deep circular trenches. Then, $In_xGa_{1-x}As$ (x~0.06) layer has been grown on such substrate by LPE. It is noticing worthy that no InGaAs buffer is used in this case. The layer grew inwards from the side wall of the trench forming a bridge over the trench. Some growth over the mask outside the trench area was observed as well. Analysis of the layer surface revealed presence of dislocated zone with etch pits density ~ 10^6 cm^{-2} only above the small area where the layer was in direct contact with the GaAs substrate. The rest of the layer, having the diameter above 1 mm, was of very high quality with dislocation density below 10^4 cm^{-2}, so it could be used as substrate for further deposition of device layers. Unfortunately, the technology presented has been tested only for very low In concentrations (and for very high In content when InAs instead of GaAs was used as the substrate [52]). Thus, more research is needed to study how this procedure would work for the heteroepitaxial structures with large lattice mismatch. Moreover, the question about quality of coalescence of the layers grown from the opposite walls of the trench seems still to be open. Despite that, the technology of LPE growth of

bridge layers over the trenches seems to be very promising due to its simplicity, very high efficiency and high quality of layers produced.

Finally, let us present the method of lateral overgrowth that has received much attention recently, namely the pendeo- (from the Latin: to *hang* or to be *suspended*) epitaxy (PE). To grow PE GaN layers, a thin AlN wetting layer and GaN buffer are grown first on an available substrate as shown in Figure 15(a). Next, trenches deep enough to reach the substrate surface (or even slightly deeper) are etched in the structure. The bottoms of trenches and top surfaces of GaN columns are then covered by a suitable masking film, so GaN column side walls are the only surfaces exposed for subsequent GaN regrowth. During pendeo-epitaxy the GaN layers overflow the trenches growing laterally from the column side walls [see Fig. 15(b)]. Also some vertical growth takes place followed by lateral growth over the mask covering the top of GaN mesas. If long enough growth time is given the PE layers starting from adjacent seeds merge at the fronts marked "A" and "B" in Fig. 15(c), so continuous PE GaN layer is formed. As mentioned before, dislocations thread in the GaN buffer along the c-axis (i.e. perpendicular to the surface). Thus, only a very small part of them intersect the side wall of GaN columns and propagate into PE GaN layer. Therefore, the regrown material contains four-to-five orders of magnitude lower density of dislocations than that in the buffer [53]. Moreover, in contrary to the ELO case, also the dislocations originally present in the buffer (marked as TDs in Fig. 15) are prevented from reaching the PE layer if the GaN columns are capped by the mask. Thus, in principle, density of dislocations should be reduced over the whole area of the substrate and the need to locate devices only in the laterally overgrown parts of the structures (see Section 3) could be eliminated.

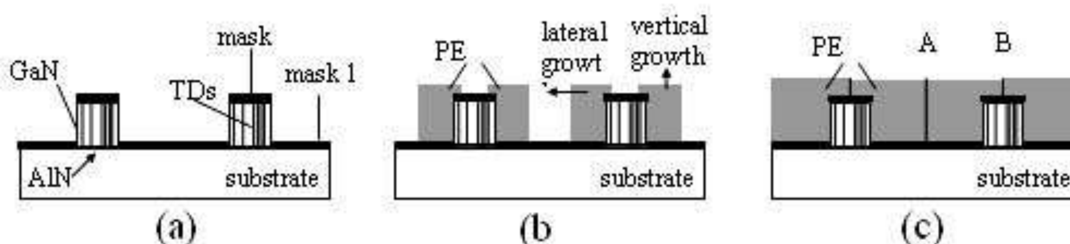

Fig.15. Schematic of the process steps for pendeo-epitaxy of GaN: (a) etching of elongated columns in GaN buffer layer followed by masking of the substrate (mask 1) and the top column surfaces (mask 2); (b) epitaxial growth of GaN starts from exposed side walls of GaN columns and proceeds laterally to fill the trenches; also some vertical growth occurs; (c) PE layers merge over the trenches (seam A) and over the capped GaN columns (seam B), so continuous PE GaN film is formed. TDs are the dislocations threading to the surface of the GaN column.

The PE technique in its version shown in Fig. 15 has been used by Chen et al. to grow by MOVPE GaN layers on SiO_2 masked sapphire substrates [54]. Studies of the layers with the use of transmission electron microscopy have proved that laterally overgrown parts of the layers are nearly dislocation-free. However, new dislocations have been found at the fronts (marked as "A" and "B" in Fig. 15) where the layers merge as well as over the edges of masked GaN columns. In the light of what has been written in Section 4.1 above, this finding is not surprising. Most probably interaction of the laterally

overgrown parts of the layers with the SiO_2 mask has occurred leading to their relative misorientation and defects creation at the coalescence fronts. Thus, this is the same phenomenon as that we have discussed already and which is illustrated in Fig. 10.

These results as well as the whole discussion in Section 4 of this review clearly show that properties of laterally overgrown layers are strongly influenced by the presence of a mask. In particular, the strain introduced by the mask and "poisoning" by impurities diffusing out from the mask at high temperature have negative impact on quality of the layers. Therefore, the processes are needed in which layers could be grown laterally without any masking film. It is important to note that each mask requires additional technological steps. Thus, maskless version of selective epitaxy would result in significant simplification of the whole procedure, which is especially important if the growth process under development is to be applied on industrial scale. Zheleva et al. have found that under proper MOVPE conditions neither GaN nor free Ga do accumulate on 6H-SiC (0001) surface [53]. Thus, the pendeo-epitaxy of GaN without mask between the GaN columns (mask 1 in Fig. 15) became possible by replacement of sapphire by SiC. As before, PE growth started from the side walls of the GaN columns and proceeded laterally at some distance from the SiC surface. Transmission electron microscopy showed that neither tilting nor low angle tilt boundary were present at the coalescence boundary over the trench [seam "A" in Fig. 15(c)]. However, tilting of 0.2^{o} and defects at the seam "B" were still found in the portion of the coalesced GaN layer, which interacted with the mask covering the GaN column [55]. This tilt can be further eliminated if completely mask-free PE process (i.e. without masks 1 and 2) is employed as has been reported for GaN [53] and AlGaN [56] on SiC systems. Then, defect-free coalescence can be obtained at both coalescence fronts [53]. The price paid for that however, is enhanced vertical growth of PE layer and free propagation into regrown GaN of TD dislocations originally present in the GaN buffer.

The next step towards commercialization of pendeo-epitaxy of GaN would be to replace SiC substrates, which are expensive and available with low diameters, by large area silicon wafers. However, direct epitaxy of GaN on Si is difficult and usually results in polycrystalline films, most likely due to the prior formation of SiN_x film on the Si surface. Therefore, Davis et al. have employed the procedure in which Si (111) substrates are first covered by epitaxial film of SiC, followed by their transfer to MOVPE system for deposition of AlN wetting layer and GaN buffer [55]. Next, they could make use of the process route elaborated earlier for PE of GaN on bulk SiC, namely, substrate etching to define GaN columns and PE regrowth. Quality of the GaN layers they obtained was quite similar to that on bulk SiC substrates. The problem however, was the thermal stress arising due to large difference of thermal expansion coefficients between subsequent layers, which resulted in cracking of the structures on cooling if the SiC transition layer was too thin.

5. Summary

Review of the epitaxial lateral overgrowth technology and of application of ELO layers as substrates with adjustable value of lattice constant is provided. Main idea behind lateral overgrowth techniques is selective epitaxy of an homoepitaxial layer on relaxed buffer having required value of lattice parameter. The seeds can be defined by patterning of the mask covering the buffer layer (ELO) or the growth starts from the exposed side walls of ridges etched in the buffer (PE). Selective nucleation of the layer in the narrow seeds allows to pass through information on buffer lattice spacing, while blocking all (or main

part of) defects created due to lattice misfit between the buffer and its substrate. We have shown numerous examples that this procedure works efficiently. Usually, practical realization of the idea above depends on the system considered. Quite often specific properties of materials and of growth technique used determine the way in which laterally overgrown structures are produced (*vide* the maskless pendeo-epitaxy of GaN on SiC). There are however, some basic phenomena typical for all laterally overgrown structures. These include some general rules that should be followed to obtain wide and thin laterally overgrown layers (i.e. choice of optimal direction of the seeds, high quality of the buffer, low growth rate, use of doping to enhance lateral growth, etc.). Efficient filtration of dislocations originally present in the buffer is well evidenced in all laterally overgrown structures. Tilt of wings caused by their interaction with the mask underneath is commonly observed both in ELO and PE layers independently on the growth technique used. If the tilt angle is small the accompanied strain can be accommodated elastically (i.e. GaAs on GaAs ELOs). Otherwise, arrays of dislocations creating low angle boundaries appear above the mask edges (i.e. the case of GaN ELO structures). Tilting of laterally grown parts of the layer leads to generation of new defects at the coalescence front where two layers grown from neighboring seeds and having opposite tilt direction merge. Growing the layers standing free above the mask seems to be the best way to improve quality of the coalescence front, although there are no general recipes how to grow such structures. Thermal strain being due to different expansion coefficients of subsequent layers is also commonly found in laterally overgrown heterostructures. However, if the layer is attached to the buffer through the narrow seeds only, this strain is usually much smaller than in reference planar structures.

It is difficult to predict how the lateral overgrowth technology will develop in the future. From scientific point of view there are still many questions to be answered. In particular, identification of microscopic interaction of ELO wings with the mask, understanding of mechanisms leading to bending of dislocations threading through the seed in ELO and many other issues require further work. Basic crystal growth research in needed to increase width of laterally overgrown layers, to improve quality of coalescence fronts, to develop technology of lateral overgrowth of ternary layers on binary substrates and to simplify the whole growth procedure according to industrial standards. Application of laterally overgrown layers will depend on progress of these studies. Growth technology must be significantly simplified for wide application of laterally overgrown substrates. Market demands for novel semiconductor devices will decide if and which techniques of lateral epitaxy find their permanent position in industrial practice. Nowadays there is a large demand for group III nitrides substrates, so lateral overgrowth of these compounds is mostly studied in many laboratories world-wide. Probably, importance of lateral overgrowth of “traditional” III-V ternary substrates will increase in the nearest future.

ACKNOWLEDGEMENTS

The author thanks D. Dobosz, J. Domagala and M. Godlewski from Institute of Physics PAS, Warsaw, A. Piotrowska, T.T. Piotrowski, E. Kaminska, E. Papis from Institute of Electron Technology, Warsawa, Poland, T. Tuomi and R. Rantamaki from Helsinki University of Technology, Helsinki, Finland and A. Rocher from CEMES-CNRS, Toulouse, France for their contribution to the presented experimental results. This work is partly supported by the Polish Committee for Scientific Research under the grant No. 3T08A 021 26.

This paper was prepared on a basis of an invited talk presented during Polish-Syrian Workshop on Semiconductor Science held in Lattakia, Syria in May 2004. The author thanks the Organizers for their hospitality and good organization of the Workshop.

REFERENCES:

1. L. Jastrzebski, J.F. Corboy, R. Soydan, J. Electrochem. Soc. 136 (1989) 3506, and references therein.
2. S. Nakamura, M. Senoh, S. Nagahama, N. Iwasa, T. Yamada, T. Matsushita, H. Kiyoku, Y. Sugimoto, T. Kozaki, H. Umemoto, M. Sano. K. Chocho, Jpn. J. Appl. Phys. 36 (1997) L1568.
3. J.C. Brice: The growth of crystals from liquids (North-Holland, Amsterdam, 1973).
4. T. Nishinaga Cryst. Prop. Prep. 31 (1991) 92.
5. R.J. Matyi, H. Shichijo, T.M. Moore, H-L. Tsai, Appl. Phys. Lett. 51 (1987) 18.
6. J.T. Torvik, J.I. Pankove, E. Iliopoulos, H. M. Ng, T. D. Moustakas, Appl. Phys. Lett. 72 (1998) 244.
7. G. Bacchin, T. Nishinaga, J. Cryst. Growth 208 (2000) 1.
8. H. Tang, J.A. Bardwell, J.B. Webb, S. Moisa, J. Fraser, S. Rolfe, Appl. Phys. Lett. 79 (2001) 2764.
9. Z.R. Zytkiewicz, Cryst. Res. Technol. 34 (1999) 573.
10. K. Hiramatsu, A. Usui, in: J.H. Edgar, S. Strite, I. Akasaki, C. Wentzel (Eds.), GaN and Related Semiconductors, EMS Datareview Series No. 23 INSPEC (IEE, London 1999) p. 440.
11. S. Sakawa, T. Nishinaga, J. Cryst. Growth 115 (1991) 145.
12. D. Dobosz, Z.R. Zytkiewicz, E. Papis, E. Kaminska, A. Piotrowska, J. Cryst. Growth 253 (2003) 102.
13. D. Dobosz and Z.R. Zytkiewicz, Int. J. Materials and Product Technology 22 (2005) 50.
14. Y.S. Chang, S. Naritsuka, T. Nishinaga, J. Crystal Growth 174 (1997) 630.
15. Y.S. Chang, S. Naritsuka, T. Nishinaga, J. Crystal Growth 192 (1998) 18.
16. Z. Yan, S. Naritsuka, T. Nishinaga, J. Crystal Growth 198/199 (1999) 1077.
17. Y. Liu, Z.R. Zytkiewicz and S. Dost, J. Cryst. Growth 275 (2005) E893.
18. Y.C. Liu, Z.R. Zytkiewicz and S. Dost J. Cryst. Growth 265 (2004) 341.
19. Z. Yan, S. Naritsuka, T. Nishinaga, J. Crystal Growth 209 (2000) 1.
20. Z.R. Zytkiewicz, D. Dobosz, M. Pawlowska, Semicond. Sci. Technol. 14 (1999) 465.
21. B. Beaumont, S. Haffouz, P. Gibart, Appl. Phys. Lett. 72 (1998) 921.
22. Z.R. Zytkiewicz, J. Domagala, Appl. Phys. Lett. 75 (1999) 2749.
23. R. Rantamaki, T. Tuomi, Z.R. Zytkiewicz, D. Dobosz, P.J. McNally, J. Phys. D 32 (1999) A114.
24. S. Sakawa, T. Nishinaga, Jpn. J. Appl. Phys. 31 (1992) L359.
25. B-Y. Tsaur, R.W. McClelland, J.C.C. Fan, R.P. Gale, J.P. Salerno, B.A. Vojak, C.O. Bozler, Appl. Phys. Lett. 41 (1982) 347.
26. P.O. Hanson, A. Gustafsson, M. Albrecht, R. Bergmann, H.P. Strunk, E. Bauser, J. Cryst. Growth 121 (1992) 790.
27. T.S. Zheleva, O-H. Nam, M.D. Bremser, R.F. Davis, Appl. Phys. Lett. 71 (1997) 2472.
28. Z. Yu, M.A.L. Johnson, T. Mcnulty, J.D. Brown, J.W. Cook, Jr., J.F. Schetzina, MRS Internet J. Nitride Semicond. Res. 3 (1998) 6; http://nsr.mij.mrs.org/3/6/.
29. S. Nakamura, M. Senoh, S. Nagahama, N. Iwasa, T. Yamada, T. Matsushita, H. Kiyoku, Y. Sugimoto, T. Kozaki, H. Umemoto, M. Sano, K. Chocho, Jpn. J. Appl. Phys. 36 (1997) L1568.
30. S. Nakamura, M. Senoh, S. Nagahama, N. Iwasa, T. Yamada, T. Matsushita, Y. Sugimoto, H. Kiyoku, Jpn. J. Appl. Phys. 36 (1997) L1059.

31. P. Kozodoy, J.P. Ibbetson, H. Marchand, P.T. Fini, S. Keller, J.S. Speck, S.P. DenBaars, U.K. Mishra, Appl. Phys. Lett. 73 (1998) 975.
32. G. Parish, S. Keller, P. Kozodoy, J.P. Ibbetson, H. Marchand, P.T. Fini, S.B. Fleischer, S.P. DenBaars, U.K. Mishra, E.J. Tarsa, Appl. Phys. Lett. 75 (1999) 247.
33. Z.R. Zytkiewicz, J. Domagala, D. Dobosz, J. Bak-Misiuk, J. Appl. Phys. 84 (1998) 6937.
34. Z.R. Zytkiewicz, J. Domagala, D. Dobosz, J. Bak-Misiuk, J. Appl. Phys. 86 (1999) 1965.
35. Z.R. Zytkiewicz, J. Domagala, D. Dobosz, Mat. Res. Soc. Symp. Proc. 570 (1999) 273.
36. R. Rantamäki, T. Tuomi, Z.R. Zytkiewicz, D. Dobosz, P.J. McNally, D. Danilewsky, Mat. Res. Soc. Symp. Proc. 570 (1999) 181.
37. R. Rantamaki, T. Tuomi, Z.R. Zytkiewicz, J. Domagala, P.J. McNally, D. Danilewsky, J. Appl. Phys. 86 (1999) 4298.
38. R. Rantamäki, T. Tuomi, Z.R. Zytkiewicz, P.J. McNally, D. Danilewsky, J. X-ray Sci. Technol. 8 (2000) 277.
39. P. Fini, H. Marchand, J.P. Ibbetson, S.P. DenBaars, U.K. Mishra, J.S. Speck, J. Cryst. Growth 209 (2000) 581.
40. A. Sakai, H. Sunakawa, A. Usui, Appl. Phys. Lett. 73 (1998) 481.
41. P. Fini, A. Munkholm, C. Thompson, G.B. Stephenson, J.A. Eastman, M.V. Ramana Murty, O. Auciello, L. Zhao, S.P. DenBaars, J.S. Speck, Appl. Phys. Lett. 76 (2000) 3893.
42. Z.R. Zytkiewicz, J. Domagala, D. Dobosz, J. Appl. Phys. 90 (2001) 6140.
43. P. Fini, L. Zhao, B. Morgan, M. Hansen, H. Marchand, J.P. Ibbetson, S.P. DenBaars, U.K. Mishra, J.S. Speck, Appl. Phys. Lett. 75 (1999) 1706.
44. H. Miyake, M. Yamaguchi, M. Haino, M. Motogaito, K. Hiramatsu, S. Nambu, Y. Kawaguchi, N. Sawaki, Y. Iyechika, T. Maeda, I. Akasaki, MRS Internet J. Nitride Semicond. Res. 5S1 (2000) W2.3; http://nsr.mij.mrs.org/5S1/W2.3/.
45. I. Kidoguchi, A. Ishibashi, G. Sugahara, Y. Ban, Appl. Phys. Lett. 76 (2000) 3768.
46. S.F. Fang, K. Adomi, S. Iyer, H. Morkoc, H. Zabel, C. Choi, N. Otsuka, J. Appl. Phys. 68**,** R31 (1990) and references therein.
47. N.Lucas, H.Zabel, H.Morkoc, H.Unlu, Appl. Phys. Lett. 52, 2117 (1988).
48. T.S. Zheleva, W.M. Ashmawi, K.A. Jones, Phys. Stat. Sol. (A) 176 (1999) 545.
49. Y. Suzuki, T. Nishinaga, Jpn. J. Appl. Phys. 29 (1990) 2685.
50. I. Silier, A. Gutjahr, N. Magel, P.O. Hansson, E. Czech, M. Konuma, E. Bauser, F. Banhart, R. Kohler, H. Raidt, B. Jenichen, J. Cryst. Growth 166 (1996) 727.
51. S. Iida, Y. Hayakawa, T. Koyama, and M. Kumagawa, J. Cryst. Growth **200** (1999) 368.
52. K. Balakrishnan, S. Iida, M. Kumagawa, Y. Hayakawa, presented during 13th Int. Conf. Cryst. Growth, Kyoto, 30 July-4 August 2001.
53. T.S. Zheleva, S.A. Smith, D.B. Thomson, K.J. Lithicum, P. Rajagopal, R.F. Davis, J. Electron. Mater. 28 (1999) L5.
54. Y. Chen, R. Schneider, S.Y. Wang, R.S. Kern, C.H. Chen, C.P. Kou, Appl. Phys. Lett. 75 (1999) 2062.
55. R.F. Davis, T. Gehrke, K.J. Lithicum, E. Preble, P. Rajagopal, C. Ronning, C. Zorman, M. Mehregany, J. Cryst. Growth 225 (2001) 335.
56. R.F. Davis, T. Gehrke, K.J. Lithicum, T.S. Zheleva, E.A. Preble, P. Rajagopal, C.A. Zorman, M. Mehregany, J. Cryst. Growth 225 (2001) 134.